Garcia-Gutierrez, L., Hernández-Jiménez, F., Cano-Pleite, E. & Soria-Verdugo, A. (2020). Experimental evaluation of the convection heat transfer coefficient of large particles moving freely in a fluidized bed reactor. *International Journal Of Heat And Mass Transfer*, 153, 119612.

DOI: 10.1016/j.ijheatmasstransfer.2020.119612

Experimental evaluation of the convection heat transfer coefficient of large particles moving freely in a fluidized bed reactor

L.M. Garcia-Gutierrez[a,*], F. Hernández-Jiménez[a], E. Cano-Pleite[a,b], A. Soria-Verdugo[a]

[a]*Universidad Carlos III of Madrid, Department of Thermal and Fluid Engineering, Av. de la Universidad, 30, 28911, Leganés, Madrid, Spain*

[b]*Engineering Department, CERN, Geneva, Switzerland*

**corresponding author: lmgarcia@ing.uc3m.es*

Abstract

Heat transfer is a key aspect in the performance of fluidized bed reactors. In particular, the dense phase heat transfer coefficient, which determines the heat exchanged between the bed and fuel particles, is of special relevance. This work presents a study on the heat transfer that occur when introducing pelletized particles of dry ice in a fluidized bed. The convection heat transfer coefficient is experimentally evaluated by means of the sublimation of dry ice particles using a novel methodology, which consists in a measurement system based on a macro-TGA fluidized bed and the corresponding evaluation of the acquired data. The system is capable of measuring the real time mass of the fluidized bed, which is a direct measure of the mass loss of the dry ice particles. The evaluation of such measurements allows to determine the convection heat transfer coefficient between the dry ice particles and the bed. Fixed and fluidized bed regimes, varying the excess gas velocity from -0.03 m/s up to 0.35 m/s, were tested for two different bed materials, namely Ballotini glass beads and alumina. The results of the sublimation and heat transfer coefficients are

in good agreement with values reported in the literature, confirming the reliability of the experimental and postprocessing methodologies. In general, higher gas velocities enhance the dry ice particles mixing in the bed up to a limit in which the sublimation and convection heat transfer coefficients do not further increase. Additionally, the influence of the buoyancy behaviour of the dry ice particles in the bed on the convection heat transfer coefficient is discussed. The convection heat transfer coefficient decreases substantially if the dry ice particles present a flotsam behaviour and the gas velocity is not sufficiently high to ensure a proper circulation of the particles in the whole bed.

Keywords: convection heat transfer coefficient; macro-TGA fluidized bed; heat transfer; dry ice sublimation; buoyancy effect; fuel particles.

Notation

A_s Surface area of dry ice particles [m^2].

c_{pe} Specific heat of the emulsion phase [J kg^{-1} K^{-1}].

d_{di} Dry ice particle diameter [m].

d_{dp} Average particle diameter of the bed material [m].

D_s Diameter of the surface equivalent sphere [m].

D_v Diameter of the volume equivalent sphere [m].

$D_{v,0}$ Initial diameter of the volume equivalent sphere [m].

h Convection heat transfer coefficient [W m^{-2} K^{-1}].

h_{gc} Heat transfer coefficient by gas convection [W m^{-2} K^{-1}].

h_{pc} Heat transfer coefficient by particle convection [W m^{-2} K^{-1}].

h_{rad} Heat transfer coefficient by radiation [W m^{-2} K^{-1}].

k Sublimation coefficient [kg m^{-2} s^{-1}].

k_e Thermal conductivity of the emulsion phase [W m^{-1} K^{-1}].

k_g Thermal conductivity of the gas [W m^{-1} K^{-1}].

L_{di} Dry ice particle length [m].

m Mass of a single dry ice particle [kg].

m_0 Initial mass of a single dry ice particle [kg].

m_c Surface thermal contact resistance constant [-].

m_t Total mass of dry ice particles [kg].

m_{t0} Total initial mass of dry ice particles [kg].

Nu_{gc} Nusselt number of gas convection [-].

Pr Prandtl number [-].

q Heat rate dissipated in the sublimation process [W].

R_c Thermal contact resistance [K m^2 W^{-1}].

R_p Thermal resistance to the thermal penetration layer [K m^2 W^{-1}].

Re_{mf} Reynolds number at minimum fluidization conditions [-].

RMSE Root mean square error of time between the fitting and the filtered signals [s].

t Time [s].

T Average temperature of the fluidized bed [K].

T_{su} Sublimation temperature of dry ice particles [K].

U Gas velocity [m s^{-1}].

U_{mf} Minimum fluidization velocity [m s^{-1}].

X Remaining percentage of mass of the dry ice particles [%].

X_{fin} Final percentage of mass of the dry ice particles [%].

Δh_{su} Latent heat of sublimation [kJ kg^{-1}].

Δt_{max} Maximum time deviation between the fitting and the filtered signals [s].

ε_{mf} Void fraction of the bed material at minimum fluidization conditions [-].

ρ_e Density of the emulsion phase [kg m^{-3}].

ρ_{di} Dry ice particle density [kg m^{-3}].

ψ Sphericity of the dry ice particle [-].

θ Mean emulsion residence time [s].

1. Introduction

Biomass is a promising alternative to fossil fuels for power generation and production of highly valuable chemicals [1]. Biomass can be converted via physico-chemical, biochemical and thermochemical processes. During physico-chemical processes, pressure is applied on oleaginous biomass to produce vegetable oil. Biochemical processes include digestion and fermentation, while the main thermochemical processes of biomass are combustion, gasification, pyrolysis, torrefaction, and hydrothermal liquefaction [2]. Numerous technologies can be employed in reactors for thermochemical conversion of biomass. Among them, fluidized beds are widely used due to several advantages, such as their homogeneous temperature of operation, high heat transfer and mixing coefficients, and the possibility of in-situ catalysis of chemical reactions [3]. Therefore, the effective heat transfer provided by fluidized beds is of critical importance for the thermochemical conversion of biomass [4].

The dense phase of a fluidized bed used for a thermochemical conversion process consists of the inert particles and the fluidizing agent. In fluidized bed reactors, it is important to distinguish among heat transfer between inert particles of bed material and gas phase, and heat transfer between larger particles and the dense phase. In the former group, most of the works that model heat transfer in fluidized bed units are based on the

works from Ranz & Marshall [5,6] and Gunn [7]. Ranz & Marshall [5,6] analysed the rate of evaporation of pure liquid drops, which modified the Frössling equation by including the Reynolds and Schmidt numbers. More specific to the fluidization process, Gunn [7] studied heat transfer between bed material particles and gas under fixed and fluidized bed regimes and proposed correlations for the Nusselt number based on the Reynolds number. Despite their different nature, both correlations have been applied successfully in modelling heat transfer in fluidized beds.

Regarding larger objects immersed in fluidized beds, the heat transfer between the fuel and the bed comprises three differentiated mechanisms: radiation, solid phase convection and gas phase convection; in addition to the conduction process occurring inside the fuel particle. The radiation coefficient depends on the bed temperature and the effective emissivity of the bed, which, according to Baskakov [8], is independent of the gas velocity. However, Boterill [9] found out that the contribution of radiation to the overall heat transfer is negligible for bed temperatures below 600 ºC. Several models are available in the literature to evaluate the solid phase convection coefficient. Most of these models assume that small groups of particles, called packets, move together due to the agitation of the bed induced by the ascension of bubbles [10]. The most widely used model to estimate the solid particle convection heat transfer coefficient in a fluidized bed is the surface resistance model, a refined version of the packets model according to which the solid phase convection coefficient can be determined based on the contact thermal resistance and the thermal penetration layer resistance [11]. Concerning gas phase convection, correlations for convection gas heat transfer coefficients in fluidized beds are typically obtained using the heat and mass transfer analogy by experimental measurements employing active particles [12]. Hayhurst and Parmar [12] based their study on correlations

formulated in terms of the Sherwood number, similar to the works of Ranz & Marshall [5,6]. Recently, more sophisticated experimental techniques allow to estimate and validate both heat transfer coefficients, gas-solid heat transfer and larger objects to dense bed heat transfer. Patil et al. [13] studied heat transfer in a fluidized bed combining DIA, PIV and IR techniques. These experimental results where compared to simulations by Li et al. [14], using Gunn's correlation to model gas-solid heat transfer. Chao et al. [11] proposed a model to estimate the heat transfer coefficient of spherical fuel particles immersed in a fluidized bed considering radiation, solid phase convection and gas phase convection. This model was validated with the experimental measurements conducted by Prins and Draijer [15], showing a good agreement between experimental results and model predictions.

The mixing of fuel particles in three-dimensional fluidized beds has been studied using a wide variety of experimental techniques, such as radioactive tracers [16, 17], dry ice sublimation [18, 19], magnetic tracer-particles [20], moisture released [21] and digital image analysis of the bed surface [22-24]. Concerning the mixing of fuel particles in pseudo-2D beds, the experimental techniques include emission of CO_2 by carbon-loaded porous particles [25], magnetic particle tracking [26], and digital image analysis of phosphorescent particles [27]: strontium aluminate covered particles [28-30] or simply larger particles that could be distinguished from the dense phase [16, 31]. The abovementioned experimental techniques have been employed to characterize the motion of fuel particles in fluidized beds, revealing that the fuel mixing patterns are strongly coupled to the bubble flow and present a strong similarity to the bulk solids flow pattern, although the latter could be altered by vertical segregation effects. At low fluidization velocities, fuel particles have been found to segregate to the dense bed surface [16, 22,

29, 32]. Pallarès and Johnsson [33] found that fuel particles with a fuel-to-bulk Archimedes ratio above 10^4 tend to float on the bed surface at fluidization velocities below 1.5 m/s. Moreover, Fiorentino et al. [34] observed that fuel particles have an enhanced tendency to segregate to the bed surface during drying and devolatilization processes as a result of the production of endogenous bubbles of moisture and volatile matter. Therefore, char particles and low-density fuels are more prone to exhibit a flotsam behaviour at low fluidization velocities, whereas, at high fluidization velocities, the higher circulation of bulk solids exerts a large enough drag force on the fuel particles to immerse them into the dense bed, gradually reducing the vertical segregation effect [24, 35, 36]. However, the correlations available in the literature for convection heat transfer coefficients between the dense bed and fuel particle typically consider that fuel particles are immersed in the dense bed and properly distributed throughout the whole height of the bed. Hence, the validity of these correlations for fuel particles exhibiting a flotsam behaviour due to a lower density compared to the dense bed and a low fluidization velocity should be evaluated.

The present work analyses the convection heat transfer coefficient between pelletized fuel particles and a fluidized bed through the sublimation coefficient of dry ice particles immersed in the bed, in a similar manner to Schlichthaerle and Werther [19]. That is, evaluating the mass loss of the dry ice particles with time. Schlichthaerle and Werther [19] determined the mass lost during the sublimation process in a fluidized bed measuring the CO_2 concentration at the gas exhaust. In contrast, the present work introduces a novel experimental procedure that consists in a macro-TGA fluidized bed capable of measuring the real time mass evolution of the full bed, with enough precision to detect the mass released by the dry ice particles during sublimation. The successful validation of the experimental and post-processing methodology allows a second main novelty: to extend

the study to evaluate the buoyancy effect on the fuel particles and how this affects heat transfer. During chemical and thermal conversion processes at low fluidization velocities, a flotsam behaviour of fuel particles of densities differing from that of the bed bulk may occur. Understanding the dependence of the heat transfer process on the flotsam behaviour of these particles is paramount for a correct evaluation of the heat transfer mechanisms in the fluidized bed.

2. Theory

The heat rate dissipated in the sublimation process of a dry ice particle, q, can be defined as the variation of mass of the particle multiplied by its latent heat of sublimation, Δh_{su}. This sublimation process of dry ice particles in the fluidized bed is assumed to be governed by heat transfer. Considering the low temperature of both the bed, which is operated at ambient temperature, and the dry ice particles, which remain at the sublimation temperature of CO_2, i.e., 194.7 K, radiative heat transfer can be neglected compared to convection heat transfer [9]. Therefore, an energy balance on a dry ice particle yields:

$$q = \frac{dm}{dt}\Delta h_{su} = -hA_s(T - T_{su}) \quad (1)$$

where T_{su} is the sublimation temperature of the dry ice particles, T is the average temperature of the fluidized bed, A_s is the surface area of the dry ice particles and h is the convection heat transfer coefficient between the dry ice particles and the fluidized bed. Prior to the tests in the macro-TGA, the bed temperature was measured during the sublimation of dry ice particles in similar conditions than the experiments, but with a thermocouple immersed into the bed. These measurements confirmed the negligible effect of sublimation on the bed temperature, which was an expected result due to the large

mass of bed material used compared to the mass of the dry ice particle. The bed average temperature, T, was then assumed to be ambient temperature, 293 K, for all the cases, whereas sublimation properties, T_{su} and Δh_{su} are included in Table 2.

According to the energy balance on the dry ice particle, Eq. (1), the sublimation coefficient, k, defined as the variation of mass with time per unit of area, is directly related to the convection coefficient as follows:

$$k = \frac{h}{\Delta h_{su}}(T - T_{su}) \quad (2)$$

In the present work, the dry ice particles are pelletized and thus present a cylindrical shape. Following the methodology employed by Schlichthaerle and Werther [19], the mass of the dry ice particle can be defined using the density of dry ice, $\rho_{di,}$ and the equivalent diameter of a sphere having the same volume as the particle, D_V:

$$m = \frac{\pi}{6}\rho_{di}{D_v}^3 \quad (3)$$

In a similar manner, the surface area of the pelletized particle can be defined using the diameter of the surface equivalent sphere, D_s. The sphericity of the particle, ψ, is defined as the ratio of the square of both equivalent diameters:

$$A_s = \pi {D_s}^2 \quad (4)$$

$$\psi = D_v^2/D_s^2 \quad (5)$$

The shrinking of the dry ice particles during sublimation was confirmed by recording a video of a single dry ice particle with an IR camera, allowing the assumption that sublimation occurs at the particle surface. Thus, from Eq. (3), the variation of the mass of

the particle with the diameter of the volume equivalent sphere can be determined by derivation:

$$\frac{dm}{dD_v} = \frac{\pi}{2}\rho_{di}D_v^2 \quad (6)$$

Introducing Eq. (6) into Eq. (1) and using the definition of sphericity provided in Eq. (5), an expression for the variation of the volume equivalent diameter of the sphere with time is obtained:

$$dD_v = \frac{-2h}{\rho_{di}\Delta h_{su}}\frac{1}{\psi}(T - T_{su})dt \quad (7)$$

Assuming that the sphericity of the pelletized dry ice particle and the temperature difference between the fluidized bed and the sublimation temperature are constant throughout the sublimation process [19], Eq. (7) can be integrated to derive a linear time evolution of the diameter of the equivalent sphere volume:

$$D_v(t) = D_{v,0} - \frac{2h}{\rho_{di}\psi\Delta h_{su}}(T - T_{su})t \quad (8)$$

Eq. (3) and Eq. (8) can be combined to obtain an expression of the time evolution of the mass of the dry ice particle as a function of its initial mass, density, sphericity, and the sublimation coefficient:

$$m(t)^{1/3} = m_0^{1/3} - \left(\frac{4\pi}{3}\frac{1}{\psi^3{\rho_{di}}^2}\right)^{1/3} kt \quad (9)$$

Eq. (9) can be expressed using the definition of the remaining percentage of mass, which measures the instantaneous mass of the dry ice particle divided by the initial mass, $X(t) = 100\, m(t)/m_0$, resulting in:

$$X(t) = 100\left(1 - \left(\frac{4\pi}{3}\frac{1}{m_0\psi^3{\rho_{di}}^2}\right)^{1/3} kt\right)^3 \quad (10)$$

Eq. (10) provides a direct relation between the percentage variation of mass of the dry ice particle in the fluidized bed, $X(t)$, the sublimation coefficient, k, and a constant parameter depending on the initial mass, m_0, the sphericity ψ, and density of the dry ice particle, ρ_{di}. Therefore, the sublimation coefficient can be determined by performing a cubic fitting of the time evolution of the remaining percentage of mass of the particle, $X(t)$, to Eq. (10). The sublimation coefficient can be directly obtained from this cubic fitting and, therefore, the convection heat transfer coefficient can be calculated using Eq. (2).

The validity of Eq. (10) to describe the time evolution of the remaining percentage of mass during the sublimation of a dry ice particle is obviously limited. Even though the initial condition of the process is fulfilled by Eq. (10), i.e., $t = 0 \rightarrow X = 100\ \%$, the condition of $X = 0\ \%$ at the end of the sublimation process is not accomplished. In fact, $X(t)$ can reach negative values in Eq. (10) for long enough times, which is not a physical possibility during the sublimation process. Therefore, the equation proposed by Schlichthaerle and Werther [19] for $X(t)$, Eq. (10), has a limit of validity that shall be established.

3. Experimental setup

Two bed materials with different properties (Ballotini glass beads and alumina) were employed to study their effect on the sublimation process ensuring similar operating properties. The different bed materials were used to guarantee a similar minimum fluidization velocity, U_{mf}, but given their different densities, also different particle sizes where selected accordingly. Since fluid-dynamics is affected by the bubbling, which is directly related to the excess gas velocity and the bed height, the same bed height was

used for both bed materials. During the sublimation tests, the mass of bed material is also a relevant parameter, since a high mass of bed material compared to the mass of dry ice is required to guarantee a constant bed temperature during the sublimation process due to the high thermal inertia of the bed. Therefore, to operate with the same bed height and mass of bed material using particles with different density, the reactor diameter should be different. Considering this, the reactor diameter selected for the Ballotini glass beads was 12 cm, whereas a 10.6 cm inner diameter was employed for the alumina particles, resulting in both cases in 1 kg of bed material for a bed height of 10 cm. The small difference between the diameter of the reactors would have a slight effect on the bed fluid-dynamics. The distributors were designed to guarantee a homogeneous fluidization of the whole bed and present the same hole diameter and open area. The main characteristics of the two facilities and bed materials employed for the experiments are presented in Table 1. The bulk density of each bed material was calculated prior to the design of the two different facilities to assure that the use of the same mass of inert particles resulted in the same fixed bed height in them. The minimum fluidization velocity was determined by a linear regression of the standard deviation of the pressure fluctuations in the bed, as stated by Puncochár [37], and confirmed by visual inspection and correlations from the literature [38, 39].

Table 1. Characteristics of the bed materials, facilities and distributors used for the experiments.

Bed characteristics		
Bed material	Ballotini glass beads	Alumina
Particle density [kg/m^3]	2500	3950
Average particle diameter [μm]	340 (250-425)	300 (200-400)

Bulk density [kg/m^3]	1456	1860
Specific heat [J/kg·K]	1329	765
Mass [kg]	1	1
Fixed bed height [m]	0.1	0.1
U_{mf} [m/s]	0.09	0.1
Facility: cylindrical reactor		
Reactor inner diameter [m]	0.120	0.106
Reactor height [m]	0.4	0.4
Distributor: perforated plate		
Number of holes	34	26
Hole diameter [m]	0.002	0.002
Open area [%]	1	1

The macro-TGA fluidized bed concept is based on a bed vessel installed on a precision scale PS 6000 R2 from RADWAG, which can measure a mass up to 6 kg with a resolution of 0.01 g. Pressurized air, delivered from a compression line, was used as a fluidizing agent. The mass flow rate of the air supplied was controlled by a set of valves and measured by a flowmeter SMC-PFM711 for flow rates up to 100 lpm and SMC-PF2A751 for flow rates up to 500 lpm. All the experimental parameters were monitored and stored using a NI9219 acquisition card connected to a computer with LabView®. Figure 1 shows a schematic view of the experimental facility, indicating the main components of the system.

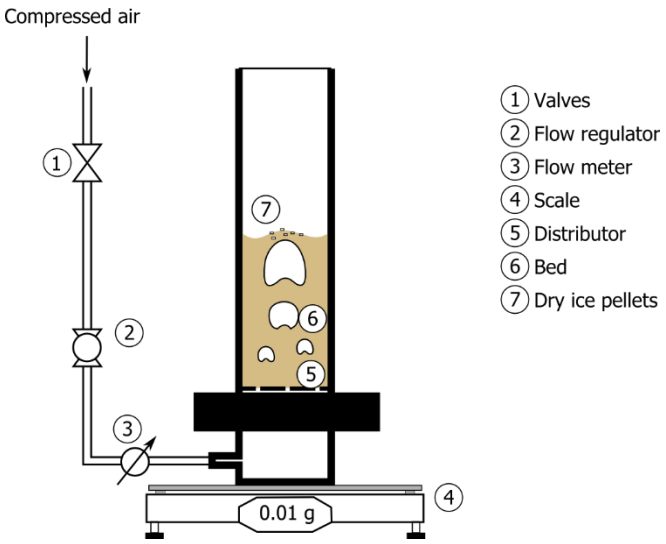

Figure 1. Schematic view of the experimental facility.

3.1. Experimental measurements

The dry ice particles have a cylindrical shape, with an average diameter of 3 mm, d_{di}, and a length of around 6 mm, L_{di}. The properties of the dry ice particles, i.e., density, sublimation temperature, and sublimation latent heat, are considered constant during the whole process. The dry ice properties were extracted from Schlichthaerle and Werther [19] and are presented in Table 2. Noteworthily, the density of the dry ice particles is similar to the bulk density of the Ballotini glass beads, but lower than the bulk density of the alumina. Considering only the densities of the bed materials and the dry ice particles, these values represent a neutrally buoyancy effect and a flotsam behaviour of the dry ice particles in the Ballotini and alumina beds, respectively, according to Soria-Verdugo et al. [29]. However, the final behaviour of the dry ice particles in the beds is strongly influenced by the drag force exerted by the fluidization agent and the bubbling behaviour, which depends on the fluidization velocity selected for the test.

Table 2. Properties of the dry ice pelletized particles.

Diameter d_{di}	**Length** L_{di}	**Density** ρ_{di}	**Sublimation temperature,** T_{su}	**Latent heat of sublimation,** Δh_{su}
3 mm	6 mm	1530 kg/m^3	194.67 K	573.02 kJ/kg

The experimental procedure consists in introducing a bunch of dry ice particles in a fluidized bed and measuring the time evolution of the mass of the system. The total initial mass of dry ice introduced for each experiment, m_{t0}, is around 10 g, ensuring enough resolution of mass variation during the process in the macro-TGA. The presence of this mass of dry ice particles in the bed, corresponding to only 1 % of the total mass of the bed, was found to be negligible for the fluid-dynamics of the bed and its minimum fluidization velocity. Firstly, the bed was fluidized with air at a given superficial gas velocity and the dry ice was extracted from the insulated box where it was stored. Secondly, the total mass of dry ice particles used for the test was determined using a laboratory scale. The precision scale was on which the reactor rested tared to measure a null mass before supplying the dry ice particles to the bed as a batch from its open top. The beginning of the test is set when the particles enter the system and their mass is registered by the scale. The time evolution of the mass measured by the precision scale on which the reactor was installed for each of the experiments were later postprocessed using Matlab®.

Five different superficial gas velocities were tested for each of the bed materials. The values of the gas velocities tested in each bed, together with their corresponding excess gas velocities are reported in Table 3. Each of the experiments presented in the table was replicated three times to ensure their repetitiveness. Note that the superficial gas velocities were chosen in such a way that the excess gas velocity, U-$U_{mf,}$ is the same for the two bed materials. This ensures a

similar visible bubble flow in the fluidized beds of Ballotini and alumina particles, which, in combination with the same bed height used in both systems, results in similar characteristics for bubbles in both fluidized beds [40]. It is also worth to mention that one of the superficial velocities corresponds to a negative excess gas velocity, which permits the determination of the convection heat transfer coefficient in fixed bed conditions. The experimental procedure for the fixed bed regime is slightly different than for the fluidized bed regime. Initially, the bed is maintained at fluidized conditions, then, the dry ice particles are supplied to the bed and the superficial gas velocity is suddenly reduced to the fixed bed conditions. This procedure ensures a homogeneous distribution of the dry ice particles inside the dense bed even for the fixed bed stage.

Table 3. Summary of the superficial gas velocities used in the experiments.

	Bed material									
	Ballotini					**Alumina**				
U_{mf} [m/s]	0.09					0.1				
U [m/s]	0.06	0.18	0.26	0.35	0.44	0.07	0.19	0.27	0.36	0.45
U-U_{mf} [m/s]	-0.03	0.09	0.17	0.26	0.35	-0.03	0.09	0.17	0.26	0.35

4. Results and Discussion

The sublimation coefficient can be directly determined from the evolution of the percentage of mass of dry ice particles with time during the sublimation process, Eq. (10). The results are presented in two parts. The first part (section 4.1 and 4.2) shows the time evolution of mass of dry ice particles sublimating in the two fluidized beds and the postprocessing of this signal to obtain the sublimation coefficients, including the analysis of the validity limits of the model proposed by Schlichthaerle and Werther [19]. In the second part (section 4.3), the results of the sublimation and convection heat transfer coefficients for the experimental

conditions of Tables 2 and 3 are derived and thoughtfully discussed.

4.1. Time evolution of the dry ice mass

Figure 2 shows the raw signal of the time evolution of the mass of dry ice particles supplied to the fluidized bed for two different superficial gas velocities using Ballotini particles as bed material. The curves presented correspond to values of the excess gas velocities, U-U_{mf}, of 0.09 and 0.26 m/s, respectively.

The instant when the pellets of dry ice are supplied to the bed can be clearly distinguished as a sharp increment of the mass up to around 10 g in Figure 2. The sublimation of the dry ice particles commences at that instant, from which the mass of the bed will decrease as time progresses. The mass curve in Figure 2 (b) shows remarkably larger fluctuations than in Figure 2 (a) due to the oscillation of the mass of the bed caused by the more vigorous fluidization for higher gas velocities. This mass fluctuation is caused by the ejection of dense phase particles forced by eruption of bubbles on the bed surface. Thus, bigger bubbles generated for increasing values of the excess gas velocity eject a greater mass of dense phase particles, resulting in a higher mass fluctuation in Figure 2 (b).

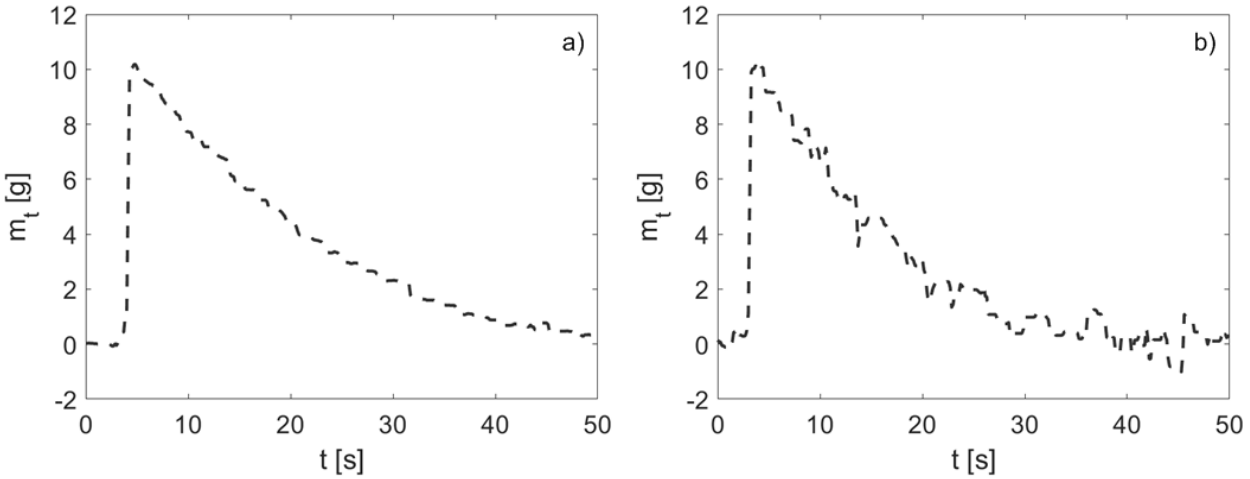

Figure 2. Time evolution of the dry ice mass for excess gas velocities of a) U-U_{mf} = 0.09 m/s and b) U-U_{mf} = 0.26 m/s. Ballotini particles as bed material.

The raw signal measured by the scale can be filtered to remove the mass fluctuation caused by the eruption of bubbles, providing a smooth curve with no abrupt variations of the mass, corresponding to the mass released by dry ice particles while sublimating in the bed. For consistency, the signals are filtered using the same methodology for all the experiments, regardless of the excess gas velocity of the bed. The applied filter consists in a moving average filter, determining the new value of each point from the average of its six closest neighbours. This moving average filter based on seven points, i.e., the six neighbours and the point considered, is applied iteratively 150 times, until the mass fluctuations caused by eruptions of bubbles are attenuated. The sampling frequency used for the measurements of the scale is 7 Hz, thus the characteristic period time of the filter, considering the 7 points used in the moving average filter, is 1 s. The number of points were selected for the filter to be capable of filtering frequencies higher than 1 Hz, such as the characteristic bubbling frequency of fluidized beds. In fact, the characteristic frequency of both beds was measured to be around 5 Hz, obtained from the power spectra of the

pressure fluctuation signal [41]. However, in addition to the filtering frequency, the number of times the moving average filter is applied iteratively on the scale signal plays also a relevant role to attain a satisfactory smoothing of the curve. The number of iterations were carefully tested, founding that 150 iterations was optimum for all cases. Further details of the filtering process can be found in Soria-Verdugo et al. [42]. This processing technique based on the mass registered by the scale and the filtering methodology has been successfully applied to analyse the mass released during biomass pyrolysis in a bubbling fluidized bed by Soria-Verdugo et al. [43] and Morato-Godino et al. [44]. The filter is applied to the time evolution of the remaining percentage of mass, *X(t),* for each test to facilitate their direct comparison. As an example, Figure 3 presents the raw evolution of *X(t)* obtained directly from the scale for the two excess gas velocities represented in Figure 2, together with the filtered signals. It can be observed in Figure 3 that the filtered signal corresponds to the global trend observed in the raw signal obtained from the scale measurement, remarkably reducing the characteristic fluctuation of mass of the raw signal, especially for the cases of high excess gas velocities.

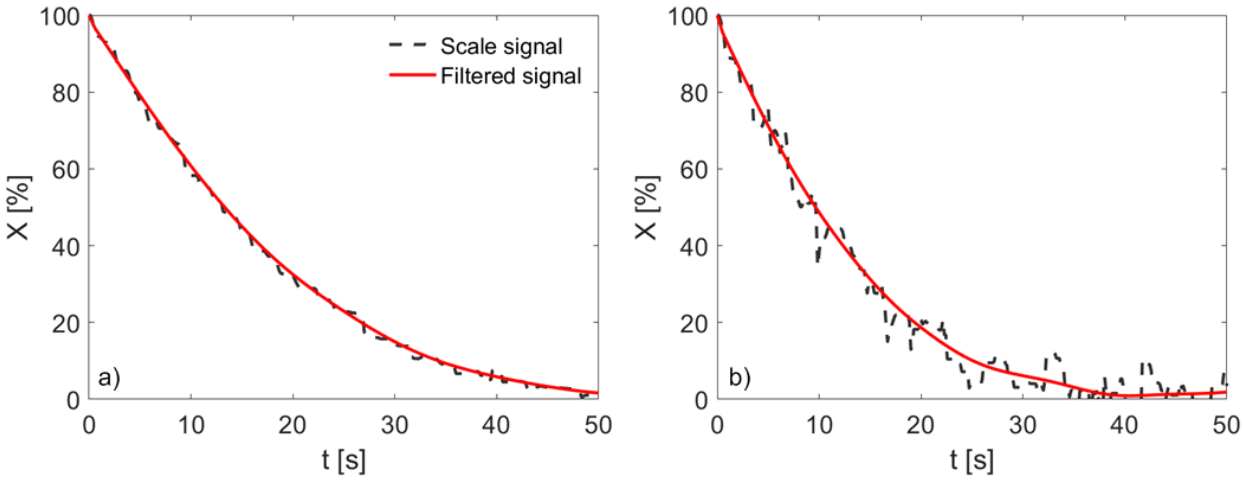

Figure 3. Raw and filtered curves of the remaining percentage of mass of dry ice for

excess gas velocities of a) U-U_{mf} = 0.09 m/s and b) U-U_{mf} = 0.26 m/s. Ballotini particles as bed material.

The mass flow rate of CO_2 released by the sublimation of the dry ice particles needs to be considered to check whether this extra excess gas may affect the fluidization regime. This can be done using the time evolution of the mass of a dry ice particle in the fluidized bed, the density of carbon dioxide and the lateral surface of the dry ice particle. For the higher excess gas velocity in Figure 3, U-U_{mf} = 0.26 m/s, the average ratio of the velocity of CO_2 released at the dry ice particle surface during the sublimation process to the superficial gas velocity is below 3.5 %. Therefore, a minor effect of Stefan flow and endogenous bubbles generated by the carbon dioxide released during the sublimation process is expected, and consequently, a negligible effect on the fluidization regime. These negligible effects of Stefan flow and endogenous bubbles are typical for the conversion of char, however, the pyrolysis or devolatilization of biomass in bubbling fluidized beds is characterized by shorter times [43, 44]. Therefore, the results obtained in this work for the convection coefficient of dry ice particles could be directly applied to char conversion, whereas they should be combined with a Stefan flow and endogenous bubbles model to be applied to devolatilizing or pyrolyzing fuel particles.

4.2. Validity of the sublimation model

The sublimation coefficient can be determined by fitting the filtered signal of the remaining percentage of mass to Eq. (10). However, as stated above, Eq. (10) is not valid for the whole sublimation process, since negative values of $X(t)$ are derived for $t >> 0$ s. Therefore, the limit of validity of Eq. (10) to describe the sublimation process should be established.

To that end, a validity analysis is carried out on the filtered signal obtained for the sublimation of dry ice particles in a Ballotini fluidized bed operated at $U\text{-}U_{mf}$ = 0.26 m/s (Figure 3 b). The final point of the sublimation process was varied from X_{fin} = 50 % to X_{fin} = 1 % in intervals of 0.5 %. For each curve, corresponding to each final point, the filtered signal was fitted to Eq. (10), obtaining the sublimation coefficient, k, as a fitting parameter. In addition, the quality of the fitting was also evaluated by determining the determination coefficient of the fitting, R^2, the time root mean squared error, RMSE, between the fitting and the filtered signal, and the maximum time deviation, Δt_{max}, of the fitting and filtered curves for specific values of X. The results of the fitting for variable final points, i.e., final values of X_{fin}, are shown in Figure 4.

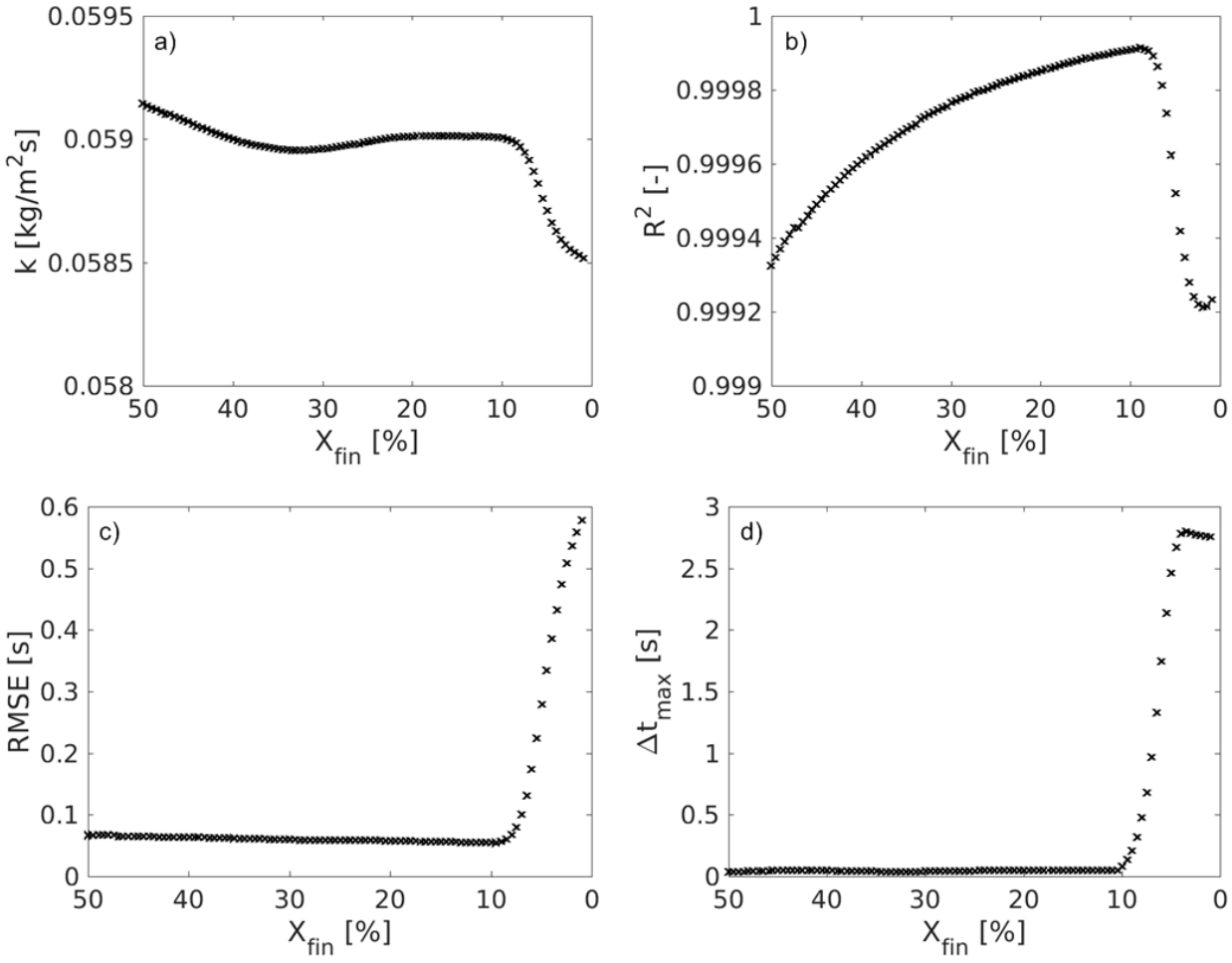

Figure 4: Results of the fitting for different final points selected for the sublimation process. a) Sublimation coefficient, b) determination coefficient, c) root mean square error of time, d) maximum time deviation.

Figure 4 (a) shows the values of the sublimation coefficient obtained from the fitting for different values of the final point selected for the sublimation process. A stable value of the sublimation coefficient is obtained for final points higher than 9 %, i.e., X_{fin} > 9 %, and sharply decreases when the final point considered is beyond 9 %. Nevertheless, despite this decrease of k for X_{fin} < 9 %, the maximum variation of the sublimation coefficient obtained varying the final point from X_{fin} = 50 % to X_{fin} = 1 % is only $5.7 \cdot 10^{-4}$ kg/m^{2}s, corresponding to a percentual variation around the stable value of 0.059 kg/m^{2}s in Figure 4 (a) lower than 1 %. Thus, the sublimation coefficient obtained from the fitting was proved to be a robust parameter. The determination coefficient of the fitting of the filtered signal to Eq. (10) is depicted in Figure 4 (b) as a function of the final sublimation point. Increasing values of R^2 are obtained when the final point changes from X_{fin} = 50 % to around X_{fin} = 9 %, unveiling that increasing the number of points of the fitting up to the limit of X_{fin} = 9 % follow the same trend described by the Eq. (10) and improves the goodness of the fitting. However, for final sublimation points lower than 9 %, the trend of R^2 changes, obtaining a reduction of the determination coefficient for decreasing values of X_{fin} in a range of around 9 % to 1 %. This reduction of R^2 for low values of X_{fin} reveals that the extra points considered for the fitting in this range does not follow the trend established by Eq. (10). In fact, for these low values of the remaining percentage of mass during sublimation, the filtered signal tends to X = 0 %, whereas Eq. (10) may lead to negative values of X, as mentioned above. Thus, the reduction of R^2 for low values of X_{fin} shows the limit of validity of Eq. (10) to describe the sublimation process.

The deviations between the fitting and the filtered signal in terms of time for specific values of the remaining percentage of mass can be observed in Figure 4 (c) and (d). Figure 4 (c) shows the root mean square error of time between the fitting and the filtered signal as a function of the considered final sublimation point. The time RMSE is uniform, even slightly decreases, when the remaining percentage of mass selected as the final point for the sublimation process decreases from 50 % to around 9 %. For lower values of the remaining percentage of mass, the RMSE increases fast, confirming the deviation between the filtered signal and the estimation of Eq. (10) for low values of X, already detected analyzing the values of R^2. The results obtained from the analysis of the time RMSE and R^2 for the validity of Eq. (10) to describe the sublimation process are quite similar. However, both the time RMSE and R^2 are global parameters for the whole process, considering information of both the beginning and the end of the sublimation process. Therefore, determining a clear limit for the validity of Eq. (10) from these parameters is complex. In contrast, the maximum time deviation between the fitting, i.e., the estimation of Eq. (10), and the filtered signal of the experimental measurement, is attained always at the end of the sublimation process, when Eq. (10) starts to differ from the experimental measurement. Thus, the maximum time deviation is a much sensitive parameter to determine divergences between the estimations of Eq. (10) and the filtered signal at the end of the process. Hence, it can be used to establish a limit for the validity of the equation. The maximum time deviation is plotted in Figure 4 (d) versus the remaining percentage of mass used as a final point for the sublimation process. The maximum time deviation is stable and low for final percentages of mass between 50 % and 10 %, increasing sharply for lower values of X_{fin}. This sharp increase of Δt_{max} corroborates the deviation between the estimation of Eq. (10) and the filtered signal at the end of the sublimation process for

low values of the remaining percentage of mass. The sharp increase of Δt_{max} contrasts with the smooth variation of both R^2 and time RMSE at this value, caused by the global character of the later parameters, which average the effect obtained at the end of the sublimation process.

Similar results to those shown in Figure 4 are obtained for different excess gas velocities and bed materials. Therefore, in view of the results obtained for the maximum time deviation of the fitting and filtered signal, the limit for the validity of Eq. (10) to describe the sublimation process of dry ice particles in a bubbling fluidized bed is established at X_{fin} = 10 %. Thus, the filtered signals for the remaining percentage of mass obtained from the mass measured by the scale will be cut at a value of X_{fin} = 10 % and the fitting will be considered only for a range of X from 100 % to 10 % in all cases. To evaluate the capability of Eq. (10) to estimate the time evolution of remaining percentage of mass during dry ice sublimation in a bubbling fluidized bed, Figure 5 shows the filtered signal of the remaining percentage of mass, obtained from the measurement of the scale, together with the cubic fitting obtained from Eq. (10), for Ballotini glass beads as bed material and excess gas velocities of U-U_{mf} = 0.09 m/s and U-U_{mf} = 0.26 m/s.

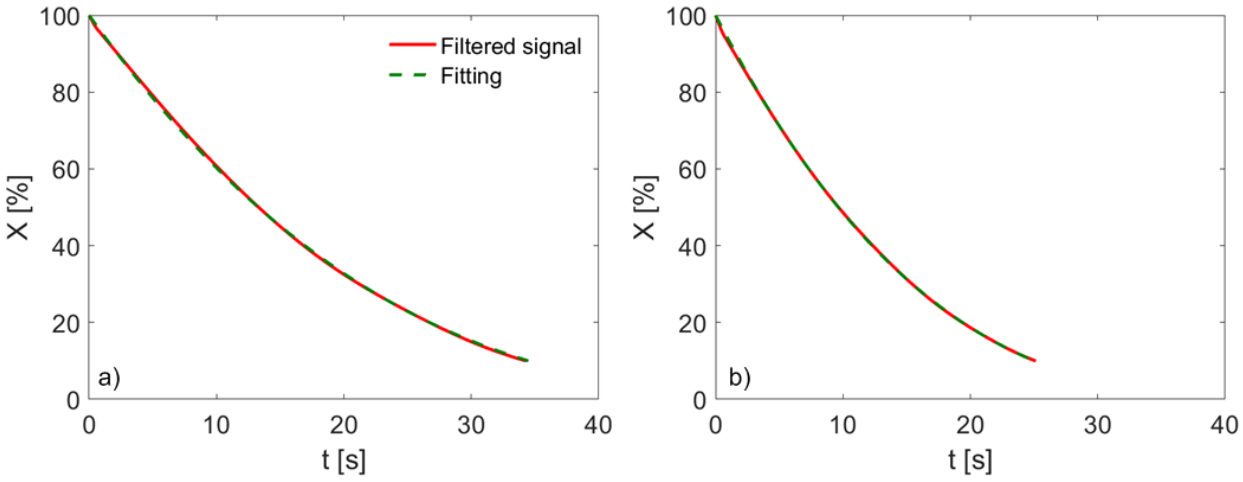

Figure 5. Filtered signal and fitting for gas velocities of a) U-U_{mf} = 0.09 m/s and b) U-U_{mf} = 0.26 m/s. Ballotini particles as bed material.

The fitting of the curves is certainly accurate in both cases, with R^2 values of these two curves of 0.9994 and 0.9999, respectively. The sublimation coefficients obtained from the fitting according to Eq. (10) for these two cases are k = 0.0482 kg/m^{2}s and k = 0.0590 kg/m^{2}s for the excess gas velocities of U-U_{mf} =0.09 m/s and U-U_{mf} =0.26 m/s, respectively. Schlichthaerle and Werther [19] proposed and used Eq. (10) to describe the time evolution of mass during sublimation of dry ice particles in bubbling fluidized beds, obtained by measuring the concentration of CO_2 of the outlet gas to infer the mass released by dry ice particles. They achieved sublimation coefficients in the range from 0.035 to 0.055 kg/m^{2}s for similar gas velocities but slightly larger dry ice particles by fitting the inferred mass released by dry ice particles to Eq. (10). Here, the complete time evolution of the mass released by dry ice particles during sublimation was directly measured, obtaining similar results to those previously reported by Schlichthaerle and Werther [19]. Therefore, the agreement of the results derived for the sublimation coefficient with the literature and the accuracy of the fitting to the experimental measurements, proved by the high values of R^2 obtained, demonstrate the reliability of the employed experimental technique and the presented filtering and fitting methodologies to determine the sublimation coefficient of dry ice particles in bubbling fluidized beds.

4.3. Sublimation and heat transfer coefficient

Once an accurate methodology to determine the sublimation coefficient from the time evolution of mass measured by the scale was presented and verified, and the validity of the dry ice sublimation model proposed by Schlichthaerle and Werther [19] was evaluated,

this section shows the influence of the gas velocity and the dense phase density on the sublimation and convection heat transfer coefficients.

Figure 6 shows the time evolution of the remaining percentage of mass after applying the filtering and fitting methodology described above during dry ice sublimation in beds of Ballotini and alumina particles for all the conditions presented in Table 3. The bed is not fluidized for negative excess gas velocities, which increases substantially the time required by the sublimation process. Thus, the motion and agitation of the bed induced by bubbles when the gas velocity is higher than the minimum fluidization velocity of the bed material enhance the sublimation of dry ice particles immersed in the dense bed, whereas in non-fluidized beds heat transfer between the dry ice particles and the bed is lower. This can be observed in Figure 6 by a significant difference between the time evolution of X in the fixed and fluidized beds. Both for Ballotini and alumina particles, the decrease of the remaining percentage of mass with time is faster for the bubbling fluidized beds, i.e., U-U_{mf} > 0 m/s, compared to the fixed beds, i.e., U-U_{mf} < 0 m/s.

The results obtained for the sublimation of dry ice particles in bubbling fluidized beds show a collapse of the X – t curves for high values of the excess gas velocities. In this situation, the bubbling behaviour of the bed is so vigorous that further increasing the gas velocity does not improve the circulation of the dry ice particles in the bed, and therefore, the heat transfer between the pelletized dry ice particles and the bed are not affected. This effect can be observed for both bed materials; however, the collapse of the filtered signals occurs for lower values of the excess gas velocities in the Ballotini fluidized bed. Differences between the two bed materials can be appreciated for an intermediate positive excess gas velocity, U-U_{mf} = 0.09 m/s, for which the sublimation process is slower in the alumina bed.

This can be attributed to the buoyancy effects on the dry ice particles immersed the bed. The lower density of Ballotini particles results in a neutrally buoyant behaviour of dry ice particles in a Ballotini bed, where the dry ice circulates through the whole bed height even for low excess gas velocities. In contrast, dry ice particles are flotsam in a bed of alumina particles, due to the higher density of the latter, restricting the motion of dry ice to a zone close to the bed surface for low excess gas velocities. This behaviour was observed during the experiments at U-U_{mf} = 0.09 m/s in the alumina bed. The different circulation of dry ice particles in the Ballotini and alumina beds for low excess gas velocities, caused by a difference on the dry ice buoyancy, involves a different heating of the particles in these two beds. Heating of dry ice particles is faster when a proper circulation of the particles is assured, i.e., in the Ballotini bed, resulting in a faster sublimation in this case. Nevertheless, the flotsam behaviour of dry ice particles in the alumina bed can be prevented by increasing the excess gas velocity, i.e., increasing the drag force on the dry ice particles. Therefore, for high values of the excess gas velocity, the filtered signals collapse independently of the ratio of densities of dry ice and the dense bed, provided that the drag force induced on the dry ice particles is high enough to overcome buoyancy forces.

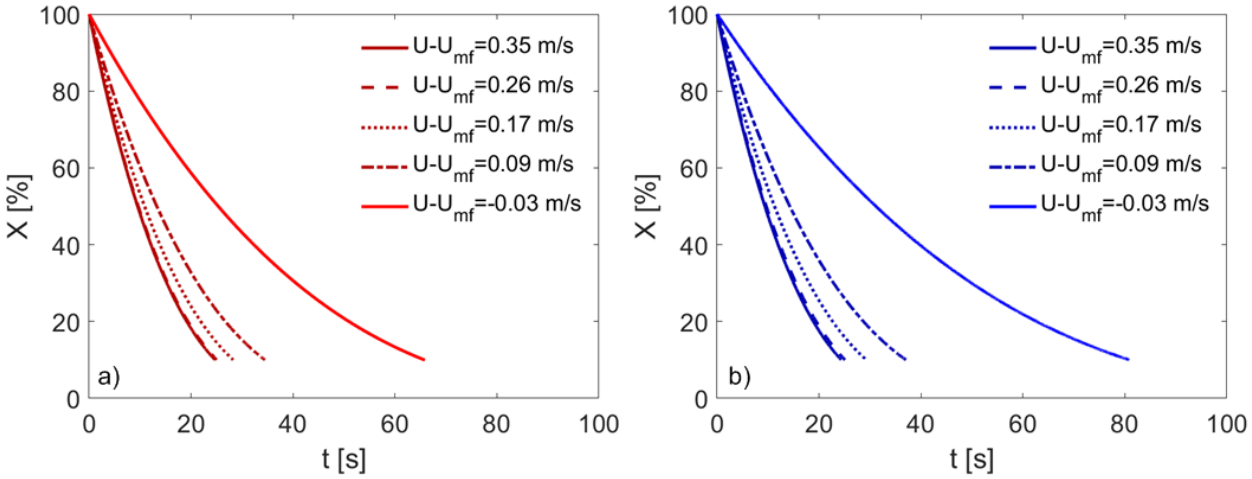

Figure 6. Fitting of the time evolution of the filtered signal of remaining percentage of mass for all excess gas velocities tested during sublimation of dry ice in a) Ballotini and b) alumina beds.

The fitting of only one of the three replicated runs for each test is shown in Figure 6 for the shake of clarity, although the results obtained for the three replicas of each operating condition will be analysed to derive the values of the sublimation and convection heat transfer coefficients. The quality of the fitting of the remaining percentage of mass of dry ice in the bed, using the filtered signals obtained from the scale, to Eq. (10) is high for all the experimental measurements conducted for each operating condition. In fact, the goodness of the fitting was checked by calculating the determination coefficient, R^2, for each fitting. The results are reported in Table 4, where the high values obtained for the determination coefficient of the fitting for all the sublimation tests conducted in bubbling fluidized beds, $R^2 > 0.996$, confirms the reliability of the experimental measurements employed to determine the mass released by dry ice particles during their sublimation in the bed and the capability of Eq. (10) to describe the sublimation process. For the sublimation tests run in fixed bed conditions, the determination coefficients of the fitting

are slightly lower, nevertheless, they are above $R^2 > 0.965$ in all cases. This slightly lower determination coefficients of the fitting for the fixed bed tests may be attributed to the stationary character of dense phase particles surrounding the dry ice particles, whose temperature would be reduced due to the heat required by the sublimation process, leading to an error in the assumption of constant temperature difference between the sublimating particles and the bed, $T\text{-}T_{su}$, required to integrate Eq. (7). Comparing the determination coefficients of the fitting obtained for the sublimation process in Ballotini and alumina fixed beds, lower values are obtained for the bed conformed by alumina particles. This is attributed to the lower heat capacity of the alumina particles compared to the Ballotini glass beads. In fact, the heat capacity is proportional to the product of its bulk density and specific heat, which is lower for the alumina particles (see Table 1). Therefore, considering the same latent heat of sublimation for the dry ice, the alumina particles surrounding a dry ice particle in a fixed bed configuration will be subjected to a higher decrease of temperature, resulting in a worse adequation to the constant bed temperature assumption of the sublimation model, leading thus to a lower fitting coefficient. Nevertheless, the obtained values of R^2, above 0.965 in all cases, are high enough to consider acceptable the fitting of the sublimation model even for fixed bed conditions.

Table 4. Determination coefficient of the fitting of the filtered signal of the mass percentage time evolution for the three replicas of dry ice sublimation tests in Ballotini and alumina beds operated at various excess gas velocities.

$U\text{-}U_{mf}$ [m/s]	R^2 [-] Ballotini bed	R^2 [-] Alumina bed
-0.03	0.9877	0.9666
	0.9829	0.9658
	0.9805	0.9650
0.09	0.9998	0.9991

	0.9996	0.9977
	0.9994	0.9972
0.17	0.9998	0.9998
	0.9990	0.9996
	0.9985	0.9992
0.26	0.9999	0.9995
	0.9988	0.9983
	0.9964	0.9979
0.35	0.9989	0.9983
	0.9983	0.9973
	0.9982	0.9971

From the fitting of the remaining percentage of mass obtained for each replica of each operating condition to Eq. (10), a value of the sublimation coefficient, *k*, is obtained as a fitting parameter. Then, the sublimation coefficient can be used to derive the convection coefficient, *h*, for each case using Eq. (2). Thus, three values of both the sublimation and the convection coefficients are obtained for each bed and excess gas velocity, corresponding to the three replicas of each experiment. Figure 7 shows the sublimation coefficient (a) and the convection heat transfer coefficient (b) for the sublimation of dry ice particles in Ballotini and alumina beds, as a function of the excess gas velocities. The dispersion of the results obtained for the different replicas is also plotted in Figure 7 for both bed materials as the maximum and minimum values obtained for all replicas of each sublimation experiment. The good repeatability of the results between the three experiments carried out for the same gas velocities confirms the reliability of the experimental and post-processing methodologies presented above for an accurate determination of the sublimation and convection heat transfer coefficients.

The trend of the sublimation and the convection heat transfer coefficients with the excess

gas velocity is the same, since *k* and *h* are related by a constant parameter depending on the latent heat of sublimation of dry ice particles and the temperature difference between the bed and the sublimating particle, Eq. (2). The sublimation and convection coefficients increase with the excess gas velocity until a certain value, above which they remain nearly constant. At a certain value of excess gas velocities, fluidization is so vigorous that increasing the gas velocity does not further improve the dry ice particle circulation. Thus, no additional increase of the convection coefficient is attained when increasing the excess gas velocity above a certain value, obtaining a constant value of *h* for high gas velocities. Significantly lower values for *k* and *h* are obtained for the fixed bed case, confirming the capability of fluidization to improve heat transfer of reacting particles. A similar tendency of the results can be observed in Figure 7 for the sublimation and convection coefficients of dry ice particles sublimating in both Ballotini and alumina beds. However, the tests conducted at $U\text{-}U_{mf}$ = 0.09 m/s resulted in different values for *k* and *h* in the bed of Ballotini and alumina particles due to the dissimilar density of these two bed materials. Lower values of the sublimation and convection coefficients were obtained for the alumina bed, where dry ice particles show a flotsam behaviour for low excess gas velocities, leading to the motion of the sublimating particles in a restricted zone of the fluidized bed close to the bed surface. In contrast, the neutrally buoyancy of dry ice particles in the lower density bed of Ballotini particles results in a proper circulation of the sublimating particles throughout the whole bed, which enhances heat and mass transfer, obtaining higher values for *k* and *h* for $U\text{-}U_{mf}$ = 0.09 m/s compared to the alumina bed. For the smooth fluidization obtained for $U\text{-}U_{mf}$ = 0.09 m/s, an increase of 23.3 % of the sublimation and convection coefficients is obtained in the Ballotini bed compared to the alumina bed due to the relevance of buoyancy effects on the dry ice particles in this denser bed.

Nevertheless, for higher excess gas velocities, i.e., $U\text{-}U_{mf} \geq 0.17$ m/s, the higher drag force induced on the dry ice particles counteracts buoyancy forces in both fluidized beds, promoting a proper mixing of sublimating particles in the bed, leading to a similar tendency for the sublimation and convection coefficients with the increasing excess gas velocity. For the vigorous fluidization obtained for $U\text{-}U_{mf} \geq 0.17$ m/s, the average results obtained for *k* and *h* are higher in the alumina fluidized bed due to the lower particle size of alumina compared to the Ballotini particles used in this work.

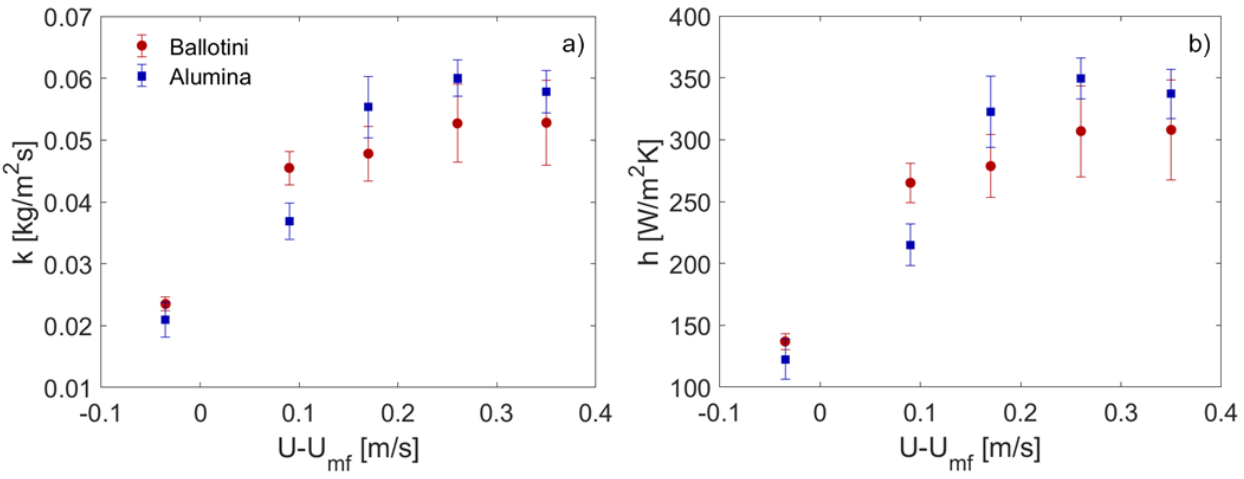

Figure 7. a) Sublimation coefficient and b) convection heat transfer coefficient as a function of the excess gas velocity in Ballotini and alumina fluidized beds.

The convection heat transfer coefficient of sublimating dry ice particles in bubbling fluidized beds of Ballotini particles operated in fluidized bed regime, i.e., $U\text{-}U_{mf} \geq 0.09$ m/s, is around 250-325 W/m^{2}K. In the alumina fluidized bed, high excess gas velocities of $U\text{-}U_{mf} \geq 0.17$ m/s results in convection coefficients for the sublimating particles of around 300-375 W/m^{2}K, slightly higher than those obtained in the Ballotini fluidized bed. However, the flotsam behaviour of dry ice particles in a bubbling fluidized bed of alumina operated at a low excess gas velocity of $U\text{-}U_{mf} = 0.09$ m/s significantly reduces the heat transfer,

obtaining convection coefficients of around 200 W/m^{2}K. For dry ice particles sublimating in fixed beds, the values obtained for the convection heat transfer coefficient are around 100-150 W/m^{2}K for both Ballotini and alumina beds. These quantitative results remark the importance of a good mixing of the reacting particles in fluidized beds to enhance heat transfer. Considering the values obtained for the convection heat transfer coefficient of the sublimating dry ice particles, an order-of-magnitude analysis can be performed considering the relevant dimensionless parameters for heat and mass transfer. In view of the heat and mass transfer Stanton numbers, it can be concluded that heat transfer is more relevant than mass transfer by one order of magnitude. This confirms the assumption that the sublimation process is governed by convection heat transfer at the particle surface.

In addition to the measurements conducted in fixed and bubbling fluidized beds, sublimation tests of dry ice particles at ambient conditions were also run. In this case, dry ice particles were place directly on the scale and the time evolution of their mass was registered, while resting stationary on the scale. The remaining percentage of mass obtained from these tests was also fitted to Eq. (10) to obtain the sublimation coefficient as a fitting parameter and the convection heat transfer coefficient from Eq. (2). These free-convection sublimation tests were replicated five times, obtaining determination coefficients, R^2, for the fitting higher than 0.99 for all cases. The value of the convection heat transfer coefficient derived for these tests is 12.0 ± 1.5 W/m^{2}K, which is similar to typical values of free convection coefficients [45-47].

4.4. Discussion

The results of the convection heat transfer coefficient of sublimating dry ice particles,

presented in Figure 7 (b) were compared to the estimation of the correlation proposed by Chao et al. [11] for the convection heat transfer coefficient between a freely moving sphere immersed in a bubbling fluidized bed of small particles. The proposed global heat transfer coefficient of the sphere moving inside the fluidized bed has three contributions, namely heat transfer by gas convection, h_{gc}, heat transfer by particle convection, h_{pc}, and heat transfer by radiation, h_{rad}. Nevertheless, radiation heat transfer can be neglected for bed temperatures below 600 ºC according to Boterill [9]. Thus, for the sublimation of dry ice particles in bubbling fluidized beds operated at ambient conditions, radiation heat transfer is not considered. The gas convection coefficient can be evaluated using the correlation proposed by Hayhurst and Parmar [12]:

$$\frac{h_{gc}d_{di}}{k_g} = \mathrm{Nu}_{gc} = 2\varepsilon_{mf} + 0.69\mathrm{Re}_{mf}^{1/2}\mathrm{Pr}^{1/3} \qquad (11)$$

where h_{gc} can be calculated as a function of the dry ice particle diameter, d_{di}, the thermal conductivity of the gas, k_g, the void fraction of the dense phase, ε_{mf}, the Reynolds number at minimum fluidization conditions, Re_{mf}, and the Prandtl number, Pr. The particle convection heat transfer coefficient considers both the thermal contact resistance, R_c, and the thermal resistance to the thermal penetration layer, R_p:

$$h_{pc} = \frac{1}{R_c + R_p} \qquad (12)$$

The thermal contact resistance, R_c, is calculated as a function of the lower and upper limit of the distribution diameter of the bed material included in Table 1, d_{dp}, the thermal conductivity of the gas, k_g, and the surface thermal contact resistance constant, m_c, as follows:

$$R_c = \frac{d_{dp}}{m_c k_g} \qquad (13)$$

where the surface heat transfer constant can be determined as:

$$m_c = 2.5\ln\left(\frac{d_{di}}{d_{dp}}\right) + 2 \qquad (14)$$

Regarding the thermal resistance to the thermal penetration layer, R_p, the following expression can be employed:

$$R_p = \frac{1}{2\sqrt{\frac{k_e \rho_e c_{pe}}{\pi\theta}}} \qquad (15)$$

where k_e, ρ_e and c_{pe} are the thermal conductivity, density and specific heat of the emulsion phase, respectively, and θ is the mean emulsion residence time, for which Chao et al. [11] proposed the following equation:

$$\theta = 0.318\left[\left(2 \cdot 10^5 d_{dp} + 24.6\right)d_{di} - 93.3 d_{dp} + 0.154\right]\left(U - U_{mf}\right)^{-0.61} \qquad (16)$$

The procedure proposed by Chao et al. [11] to determine the convection heat transfer coefficient of particles immersed in bubbling fluidized beds was followed to estimate the convection coefficient of the sublimating particles. The correlations proposed by Chao et al. [11] consider a spherical shape for the particle immersed in the bed. However, the dry ice particles are cylindrical, and their size is reduced during the sublimating process. Therefore, an average diameter of an equivalent sphere with the same volume as the cylindrical dry ice particles during the whole process is used for the estimations. The experimental results and the upper and lower limit predictions of the correlation proposed by Chao et al. [11] are presented in Figure 8 (a) and Figure 8 (b) for the Ballotini and alumina bed materials, respectively, as a function of the excess gas velocities shown in

Table 3. The limits correspond to the upper and lower diameters of the bed particles tested.

For both bed particles, the experimental results are between the correlation limits for excess gas velocities which ensure a proper mixing of the dry ice particles in the whole bed, i.e., $U\text{-}U_{mf} \geq 0.09$ m/s for the Ballotini bed and $U\text{-}U_{mf} \geq 0.17$ m/s for the alumina bed. The experimental results of the convection coefficient of dry ice particles immersed in bubbling fluidized beds derived in this work were also compared to convection coefficients estimated by different correlations available in the literature [48-53] for heat transfer between a fluidized bed and a horizontal tube. These correlations were used as a limiting case of a large cylinder, considering the average diameter of the dry ice particles. Even though the estimated values of h obtained from the correlations vary widely, the experimental results obtained in this work are within the range of variation of the predictions obtained from the correlations [48-53].

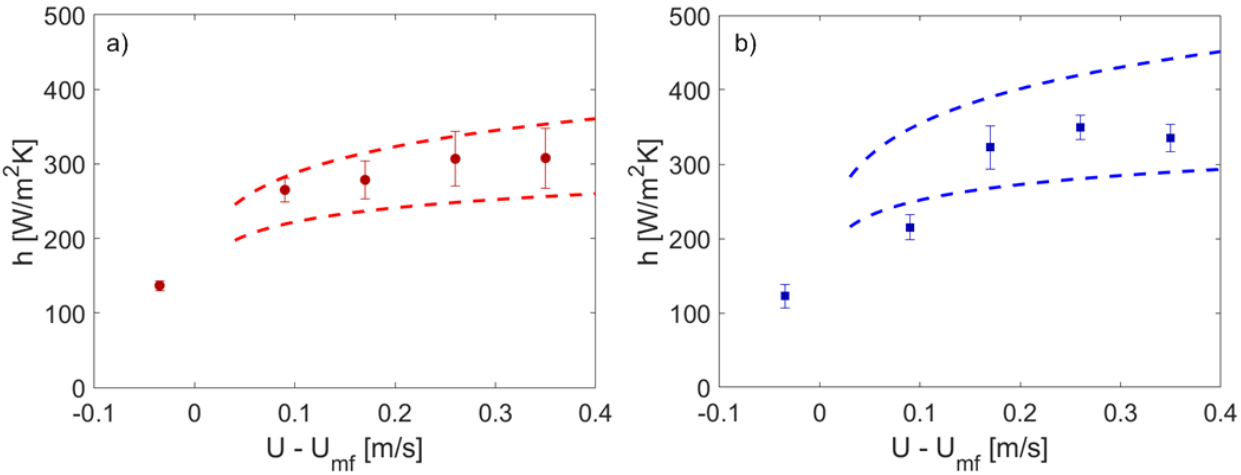

Figure 8. Comparison of the convection heat transfer coefficient between the experimental data and upper and lower limit of Chao et al. [11] correlation for a) Ballotini particles and b) alumina particles.

Interestingly, the model is not capable of correctly predicting the convection heat transfer

coefficient for low excess gas velocities of $U\text{-}U_{mf}$ = 0.09 m/s in the fluidized bed conformed by alumina particles (Figure 8 (b)). In fact, the values of the convection heat transfer derived from the experimental measurements at $U\text{-}U_{mf}$ = 0.09 m/s in the alumina bed are below the lower limit established by the correlation of Chao et al. [11]. This deviation of the estimation of the convection coefficient is again attributed to the flotsam character of the dry ice particles in the alumina bed, which results in the motion of sublimating particles in a zone of the bed close to the surface. In consequence, the correlation overestimates the convection heat transfer coefficient of these dry ice particles since the correlation is conceived for spheres properly mixed in the whole fluidized bed. This result is of particular importance for applications with low-density fuels or particles exhibiting a flotsam behaviour when immersed in fluidized beds operated at low gas velocities. For instance, for the conversion of biomass char, whose density can be substantially reduced compared to the unreacted biomass [54]. In these cases, the correlations available in the literature assume that the particles are fully immersed and properly mixed in the bed, and thus, the prediction of the correlations for h would not be valid for sufficiently low excess gas velocities. In fact, the specific case of a flotsam reactive particle in combination with a low superficial gas velocity, even above minimum fluidization conditions, dramatically reduces the heat transfer. The overprediction of the convection heat transfer coefficient obtained from correlations would lead to an overestimation of the heat transfer of these low-density particles in the bed, which may result in an undesired performance of the reactor and eventually in a collapse of the system. Therefore, it is of paramount importance to ensure a good circulation of the reactive particles in the bed to assure a correct performance of the reactor, or to guarantee a proper estimation of the heat transfer of low-density particles in a bed operated at low velocity, considering the relevant buoyancy effects and their effect

on the motion and heat transfer of the particles in these cases.

5. Conclusions

The heat transfer for a particle immersed in a fluidized bed were evaluated from the sublimation process of pelletized particles of dry ice in a macro-TGA bubbling fluidized bed by means of a non-intrusive experimental technique. Several excess gas velocities, including a fixed bed and several cases of fluidized bed regimes were investigated in this work, including also two different bed materials, in which the dry ice particles exhibit a neutral and a flotsam behaviour.

The sublimation process is accelerated when the excess gas velocity increases up to a certain value. Sufficiently high excess gas velocities guarantee a vigorous fluidization of the bed, inducing a good mixing of the dry ice particles in the whole bed. This results in a very slight impact of the gas superficial velocity on the sublimation process. The sublimation coefficient is directly linked with the convection heat transfer coefficient, showing similar values for both bed materials provided that a proper circulation of the dry ice particles throughout the whole bed height occurs. However, when the dry ice particles exhibit a flotsam behaviour due to the higher density of the bed material, e.g., alumina particles, and a less vigorous fluidization regime is imposed to the bed, the sublimation coefficient and the convection heat transfer coefficient notably decrease.

Finally, the experimental results obtained for the convection heat transfer coefficient are in very good agreement with values available in the literature for well mixed conditions, that is, when buoyancy effects are negligible, either for a similar density of the particles and the dense bed or for a high excess gas velocity that exerts a high drag force capable

of counteracting buoyancy forces. The agreement between the experimental results and the estimations of correlations confirms the reliability of the proposed experimental technique and the post-processing methodology and its potential to study further conditions. Additionally, the results revealed the need to carefully address fluidized bed performance for chemical and thermal conversion processes where low-density fuels are present, as their flotsam behaviour could dramatically worsen the heat transfer between the fuel particles and the bed.

References

[1] F.B. Ahmad, Z. Zhang, W.O.S. Doherty, I.M. O'Hara. The outlook of the production of advanced fuels and chemicals from integrated oil palm biomass biorefinery. Renewable and Sustainable Energy Reviews 119 (2019) 386-411.

[2] P. Basu. Biomass gasification and pyrolysis. Practical design and theory. Elsevier Inc. (2010).

[3] D. Kunii, O. Levenspiel. Fluidization Engineering, 2nd Ed. Butterworth-Heinemann, Boston (1991).

[4] M. Fattahi, S.H. Hosseini, G. Ahmadi, A. Parvareh. Numerical simulation of heat transfer coefficient around different immersed bodies in a fluidized bed containing Geldart B particles. International Journal of Heat and Mass Transfer 141 (2019) 353-366.

[5] W.E. Ranz, W.R. Marshall, Evaporation from drops – Part 1. Chemical Engineering Progress 48 (1952) 141-146.

[6] W.E. Ranz, W.R. Marshall, Evaporation from drops – Part 2. Chemical Engineering

Progress 48 (1952) 173-180.

[7] D.J. Gunn, Transfer of heat or mass to particles in fixed and fluidised beds, International Journal of Heat and Mass Transfer 21(4) (1978) 467-476.

[8] A.P. Baskakov. Processes of Heat and Mass Transfer in Fluidized Bed, Metallurgy Press, Sverdlovsk (1978).

[9] J.S.M. Botterill. Fluid-bed Heat Transfer. Academic Press, London (1975).

[10] H.S. Mickley, D.F. Fairbanks. Mechanism of heat transfer to fluidized beds. AIChE Journal 1 (3) (1955) 374-384.

[11] J. Chao, J. Lu, H. Yang, M. Zhang, Q. Liu. Experimental study on the heat transfer coefficient between a freely moving sphere and a fluidized bed of small particles, International Journal of Heat and Mass Transfer 80 (2015) 115-125.

[12] A.N. Hayhurst, M.S. Parmar. Measurement of the mass transfer coefficient and Sherwood number for carbon spheres burning in bubbling fluidized bed. Combustion and Flame 130 (4) (2002) 361-375.

[13] A.V. Patil, E. Peters, V.S. Sutkar, N. Deen, J. Kuipers, A study of heat transfer in fluidized beds using an integrated DIA/PIV/IR technique. Chemical Engineering Journal 259 (2015) 90-106.

[14] Z. Li, T.C.E. Janssen, K.A. Buist, N.G. Deen, M. van Sint Annaland, J.A.M. Kuipers, Experimental and simulation study of heat transfer in fluidized beds with heat production, Chemical Engineering Journal 317 (2017) 242-257.

[15] W. Prins, W. Draijer. Heat transfer to immersed spheres fixed or freely moving in a

gas-fluidized bed, in: W.P.M. van Swaaij, N.H. Afgan (Eds.). Heat and mass transfer in fixed and fluidized beds. Hemisphere Publishing Corp. Washington (1986) 317-331.

[16] G.M. Rios, K. Dang Tran, H. Masson. Free object motion in a gas fluidized bed. Chemical Engineering Communications 47 (1986) 247-272.

[17] F. Fotovat, J. Chaouki. Characterization of the upward motion of an object immersed in a bubbling fluidized bed of fine particles. Chemical Engineering Journal 280 (2015) 26-35.

[18] J. Bellgardt, A. Werther, A novel method for the investigation of particle mixing in gas-solid systems. Powder Technology 48 (1986) 173-180.

[19] P. Schlichthaerle, J. Werther. Influence of the particle size and superficial gas velocity on the sublimation of pure substances in fluidized beds of different sizes. Drying Technology, 18 (2000) 2217-2237.

[20] E. Sette, D. Pallarès, F. Johnsson, F. Ahrentorp, A. Ericsson, C. Johansson. Magnetic tracer-particle tracking in a fluid dynamically down-scaled bubbling fluidized bed. Fuel Processing Technology 138 (2015) 368-377.

[21] F. Niklasson, H. Thunman, F. Johnsson, B. Leckner. Estimation of solids mixing in a fluidized bed combustor. Industrial & Engineering Chemistry Research 41 (2002) 4663-4673.

[22] A. Soria-Verdugo, N. García-Hernando, J.A. Almendros-Ibáñez, U. García-Hernando. Motion of a large object in a bubbling fluidized bed with a rotating distributor. Chemical Engineering and Processing 50 (2011) 859-868.

[23] J. Olsson, D. Pallarès, F. Johnsson. Lateral fuel dispersion in a large-scale bubbling fluidized bed. Chemical Engineering Science 74 (2012) 148-159.

[24] E. Sette, T. Berdugo Vilches, D. Pallarès, F. Johnsson. Measuring fuel mixing under industrial fluidized-bed conditions – A camera-probe based fuel tracking system. Applied Energy 163 (2016) 304-312.

[25] I.N.S. Winaya, T. Shimizu, D. Yamada. A new method to evaluate horizontal solid dispersion in a bubbling fluidized bed. Powder Technology 178 (2007) 173-178.

[26] K.A. Buist, T.W. van Erdewijk, N.G. Deen, J.A.M. Kuipers. Determination and Comparison of Rotational Velocity in a Pseudo 2-D Fluidized Bed Using Magnetic Particle Tracking and Discrete Particle Modeling. AIChE Journal 61 (2015) 3199–3209.

[27] D. Pallarès, F. Johnsson. A novel technique for particle tracking in cold 2-dimensional fluidized beds – simulating fuel dispersion. Chemical Engineering Science 61 (2006) 2710-2720.

[28] A. Soria-Verdugo, L.M. Garcia-Gutierrez, S. Sánchez-Delgado, U. Ruiz-Rivas. Circulation of an object immersed in a bubbling fluidized bed. Chemical Engineering Science 66 (2011) 78-87.

[29] A. Soria-Verdugo, L.M. Garcia-Gutierrez, N. García-Hernando, U. Ruiz-Rivas. Buoyancy effects on objects moving in a bubbling fluidized bed. Chemical Engineering Science 66 (2011) 2833-2841.

[30] L.M. Garcia-Gutierrez, A. Soria-Verdugo, N. Garcia-Hernando, U. Ruiz-Rivas. Simulation of object motion in a bubbling fluidized bed using a Monte Carlo method.

Chemical Engineering Science 96 (2013) 26-32.

[31] K.S. Lim, P.K. Agarwal. Circulatory motion of a large and lighter sphere in a bubbling fluidized bed of smaller and heavier particles. Chemical Engineering Science 49 (3) (1994) 421-424.

[32] T.H. Nguyen T.H. and J.R. Grace. Forces on objects immersed in fluidized beds. Powder Technology 19 (1978) 255-264.

[33] D. Pallarès, F. Johnsson. Modeling of fuel mixing in fluidized bed combustors. Chemical Engineering Science 63 (2008) 5663-5671.

[34] M. Fiorentino, A. Marzocchella, P. Salatino. Segregation of fuel particles and volatile matter during devolatilization in a fluidized bed reactor – II Experimental. Chemical Engineering Science 52 (1997) 1909-1922.

[35] A.W. Nienow, P.N. Rowe, T. Chiwa. Mixing and segregation of a small proportion of large particles in gas fluidized beds of considerably smaller ones. AIChE Symposium Series 74 1978 45-53.

[36] L. Lundberg, A. Soria-Verdugo, D. Pallarès, R. Johansson, H. Thunman. The role of fuel mixing on char conversion in a fluidized bed. Powder Technology 316 (2017) 677-686.

[37] M. Puncochár, J. Drahos, J. Cermák, K. Selucký. Evaluation of minimum fluidization velocity in gas fluidized beds from pressure fluctuations. Chemical Engineering Communications 35 (1985) 81-87.

[38] C.Y. Wen and Y.H. Yu. A generalized method for predicting the minimum fluidization

velocity. AIChEJ 12 (3) (1966) 610-612.

[39] A. Delebarre. Revisiting the Wen and Yu equations for minimum fluidization velocity prediction. Chemical Engineering Research and Design 82 (A5) (2004) 587–590.

[40] R.C Darton, R.D. LaNauze, J.F. Davidson, D. Harrison. Bubble growth due to coalescence in fluidized beds. Transactions of the Institute of Chemical Engineering 55 (1977) 274-280.

[41] P.W. Welch. The use of a fast Fourier transform for the estimation of power spectra. IEEE Trans. Audio and Electroacustics AU-15 (1967) 70-73.

[42] A. Soria-Verdugo, A. Morato-Godino, L.M. Garcia-Gutierrez, N. García-Hernando. Pyrolysis of sewage sludge in a bubbling fluidized bed: Determination of the reaction rate. In 12th International Conference on Fluidized Bed Technology, CFB 2017 (2017a) p.707-714.

[43] A. Soria-Verdugo, A. Morato-Godino, L.M. Garcia-Gutierrez, N. García-Hernando. Pyrolysis of sewage sludge in a fixed and a bubbling fluidized bed – Estimation and experimental validation of the pyrolysis time. Energy Conversion and Management 144 (2017) 235-242.

[44] A. Morato-Godino, S. Sánchez-Delgado, N. García-Hernando, A. Soria-Verdugo. Pyrolysis of Cynara cardunculus L. samples – Effect of operating conditions and bed stage on the evolution of the conversion. Chemical Engineering Journal 351 (2018) 371-381.

[45] T.L. Bergman, A.S. Lavine, F.P. Incropera, D.P. DeWitt. Fundamentals of Heat and Mass Transfer 7th ed., John Wiley & Sons (2011).

[46] F. Kreith, M. S. Bohn. Principles of Heat Transfer 6 th ed., Brooks/Cole (2011).

[47] A.J. Chapman. Fundamentals of Heat Transfer. McMillan Publishing Company (1987).

[48] N.S. Grewal, S.C. Saxena, Heat transfer between a horizontal tube and a gas-solid fluidized bed. International Journal of Heat and Mass Transfer 23 (1980) 1505-1519.

[49] B.R. Andeen, L.R. Glicksman, Heat transfer to horisontal tubes in shallow fluidized beds. ASME-AIChe Heat Transfer Conference. St Louis, MO, 1976.

[50] W.E. Genetti, R.A. Schmall, E.S. Grimmett, The effect of tube orientation on heat transfer with bare and finned tubes in a fluidized bed. Chemical engineering progress symposium series 116 (1971) 90-96.

[51] N.I. Gelperin, V.Y. Kruglikov, V.G. Ainshtein, V.G. Ainshtein, N.I. Gelperin, Heat transfer between a fluidized bed and a surface of a single tube in longitudinal and transverse gas flow. International Chemical Engineering 6 (1966).

[52] H.A. Vreedenberg, Heat transfer between a fluidized bed and a horizontal tube. Chemical Engineering Science 9 (1958) 52-60.

[53] V. Stenberg, V. Sköldberg, L. Öhrby, M. Rydén. Evaluation of bed-to-tube surface heat transfer coefficient for a horizontal tube in bubbling fluidized bed at high temperature. Powder Technology 352 (2019) 488-500.

[54] A. Soria-Verdugo, L. von Berg, D. Serrano, C. Hochenauer, R. Scharler, A. Anca-Couce. Effect of bed material density on the performance of steam gasification of biomass in bubbling fluidized beds. Fuel 257 (2019) 116118.